Hindawi
Geofluids
Volume 2020, Article ID 8886988, 14 pages
https://doi.org/10.1155/2020/8886988

Research Article

A Comprehensive Model for Estimating Stimulated Reservoir Volume Based on Flowback Data in Shale Gas Reservoirs

Qi Chen,[1] Shaojun Wang,[2] Dan Zhu,[3] Guoxuan Ren,[4] Yuan Zhang,[1] and Jinghong Hu[1]

[1]*Beijing Key Laboratory of Unconventional Natural Gas Geology Evaluation and Development Engineering, China University of Geosciences, Beijing 100083, China*
[2]*Research Institute of Petroleum Exploration & Development, Beijing 100083, China*
[3]*The 5th Oil Production Plant, Changqing Oilfield, Xi'an 710021, China*
[4]*Leewen-Cobra International Energy (Beijing) Technology, Co., Ltd., 100084, China*

Correspondence should be addressed to Jinghong Hu; hjhwhat@163.com

Received 12 May 2020; Revised 24 July 2020; Accepted 28 August 2020; Published 9 September 2020

Academic Editor: Jinze Xu

Stimulated reservoir volume (SRV) which is generated by horizontal drilling with multistage hydraulic fracturing governs the production in the shale gas reservoirs. Although microseismic data has been used to estimate the SRV, it is high-priced and sometimes overestimated. Additionally, the effect of stress sensitivity on SRV is not considered in abnormal overpressure areas. Thus, the objective of this work is to characterize subsurface fracture networks with stress sensitivity of permeability through the shale gas well production data of the early flowback stage. The flowback regions are first identified with the flowback data of two shale gas wells in South China. Then, we measured the permeability stress sensitivity of the core after fracturing, coupled to the dynamic relative permeability (DRP) calculation to obtain an accurate and simple DRP curve. After that, a comprehensive model is built considering dynamic two-phase relative permeability function and stress sensitivity. Finally, we compared the calculated results with the microseismic data. The results show that the proposed model could reasonably predict the SRV using the flowback data after fracturing. Additionally, compared with the microseismic data, the stress sensitivity should be included, especially in the abnormal overpressure block. It is believed that this mathematical model is accurate and useful. The work provides an efficient approach to estimate stimulated reservoir volume in the shale gas reservoirs.

1. Introduction

The development of shale gas has gained increasing attention with the decline of the production from conventional reservoirs [1, 2]. Due to the ultralow permeability of shales (from 10^{-23} to 10^{-17} m^2) [3], a combination of horizontal drilling and multistage hydraulic fracturing has been widely used to SRV, which increases effective contact significantly to improve gas production from an individual well. Therefore, characterization of the stimulated reservoir volume appears to be of vital importance to manage and predict shale reservoir performance [4, 5].

While microseismic data has been extensively used to validate the stimulated reservoir volume, the SRV obtained directly from the microseismic data is generally overestimated. For example, SRV would include large unstimulated void regions by the convexity assumption [6–9]. Also, implementation of microseismic techniques in a field sometimes is not cost-effective, which limits a wide application in fields. Therefore, using early production data after hydraulic fracturing together with early flowback data of hydraulic fluids is fast becoming a key instrument in evaluating SRV [10–13], namely, transient analysis of flowback data.

Two-phase flow appears to be a classic and representative flow behavior during the flowback process after hydraulic fracturing [2, 14]. For example, a large number of production data obtained from wells in the Horn River shale show that two-phase flow was observed for every single well during the flowback process after hydraulic fracturing [15, 16]. Clarkson [17] and Williams-Kovacs and Clarkson [18] also discovered two-phase flow within 48 hours of well opening and production in the Barnett and Marcellus shales.

Similarly, the two-phase flow stage occurs in the Silurian Longmaxi Formation shale gas wells in South China after the well opening [19]. And an even greater advance in the research of production data patterns is that after processing the production data from shale gas wells in the Horn River Basin, Adefidipe et al. [20, 21] and Xu et al. [22, 23] divided the production data into two stages as early gas production (EGP) and late gas production (LGP) for the "V" shape of the relationship between the gas-water ratio (GWR) and the cumulative gas production. They believed that the EGP stage was special and worth studying because the LGP stage already had a matrix gas supply.

To take advantage of the two-phase flow characteristics during the early gas production (EGP) stage, research studies have endeavored to estimate the SRV by coupling rock physics with various types of reservoir models. For example, Ezulike et al. [24–26] integrated an explicitly determined dynamic relative permeability (DRP) function in linear dual-porosity models to explore the two-phase flowback data. The function extends the single-phase water flow equation to gas-water two-phase flow which was calculated using cumulative production data of water and hydrocarbon compounds. Clarkson et al. [17, 27, 28] initially used an improved method for coalbed methane (CBM) flow to analyze multiphase flows. They assumed that the flow of gas and water through the generated fracture network was similar to the simultaneous flow of gas and water during long-term production from fractured coal reservoirs. Later, they proposed a large number of two-phase flow models based on this assumption to quantitatively calculate multiflow data, including tight oil and tight gas, to help analyze the flow characteristics of shale gas wells which are analogous to analyzing two-phase (gas and water) CBM production. And in the follow-up research work [29–32], they verified the analysis results from the above methods by integrating various techniques, including a modified material balance equation (MBE) applied to before-breakthrough (BBT) (before gas breakthrough) single-phase rate-transient analysis (RTA) and after-breakthrough (ABT) (after gas breakthrough) multiphase rate-transient analysis (RTA).

While the aforementioned models provide insights in calculating SRV through multiflow data quantitatively, challenges of applying these models to the field remain because the Langmuir volume needs to be increased in the calculation process, which will lead to some extent uncertainty and inaccuracy. To overcome the complexity of applying these models in fields, Clarkson et al. [17, 28] and Fu et al. [33] established a linear matching curve relation to describe the straight line relationship between rate-normalized pressure (RNP) and material balance time (MBT). This is because fracture permeability and fracture volume can be obtained on the basis of the characteristics of the fitting curve. Also, Alkouh et al. [34] modified a log-log plot of RNP and RNP derivative against MBT for both the oil and gas cases and provided a straightforward approach to calculate the key fracture parameters covering fracture permeability and fracture half-length. However, the influence of fracture compressibility during the flowback process is not taken into consideration in the models, which likely leads to estimation error of the total compressibility.

However, due to some defects in the hypothesis of DRP function, a nonlinear phenomenon occurs when the model is applied to some field cases. And the phenomenon of the nonzero intercept leads researchers to question the physical properties of these problems. It may be due to the inaccuracies caused by stress sensitivity in some areas. In particular, there is abnormal overpressure in shale gas reservoirs in southern China [35], so the influence of stress sensitivity, especially for the two-phase relative permeability, has to be taken into account [36]. Moreover, all the researchers did not make a production data verification and comparison with the microseismic data.

We thus aimed to develop a stress-dependent two-phase relative permeability, which can be used to extend the existing single-phase model. Also, we proposed a new multiphase model to estimate SRV and fracture characteristics. Moreover, to verify our model, we compared the results with the microseismic data.

In this work, we first processed the production data of shale gas wells and obtain the gas-water ratio characteristics. Then, we calculated the simple and practical two-phase dynamic relative permeability (DRP) based on the production data collected in the field belonging to shale gas wells in southern Sichuan. Subsequently, the stress-strain curves of permeability are obtained by using the laboratory experiments. Finally, the material balance equation and diffusion equation are used to process the production data to derive the model, thus calculating fracture parameters. We compared the calculation results with the microseismic data to verify the rationality and accuracy of the calculation results.

2. Data Preparation

2.1. Field Data from a Typical Shale Gas Reservoir in Southern China. In this work, we selected the flowback data from two production wells located in southern China: the shale gas formations of the Lower Silurianare, a typical marine shale gas reservoir. A large number of micron-nanoscale pores are developed in the mineral grains and organic matter [37]. These pores are the main channels for shale gas storage and migration, which play an important role in improving shale gas storage performance and providing good storage space for marine shale gas accumulation and enrichment [38]. The depth of the shale gas reservoir is over 2000 m at subsurface with a formation pressure coefficient up to 2.0. The thickness of the entire shale reservoir is about 100 m with porosity ranging from 2% to 4% and matrix permeability of 0.001 mD. The production at the early stage was about $10 \sim 20 \times 10^4\ m^3/d$ with a stable production around at $5 \sim 8 \times 10^4\ m^3/d$.

The east-west anticline structure belt with few faults is arranged in the left echelon row as the main geological structure of this area [39]. This drilling platform is located at the end of the anticline structure. Although two compresso-shear faults exist around the well pad, the overall upper lateral sealing performance leads to an effective accumulation and preservation of shale gas [37, 38]. Figure 1 shows the layout of the horizontal well group. Due to the low quartz content in the high-quality shale segment at the bottom of the

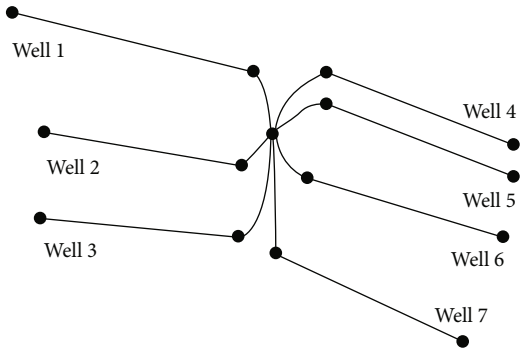

Figure 1: Well pad schematic. Seven MFHWs drilled in the southern Sichuan Basin.

Longmaxi Formation, natural fractures are not developed throughout the reservoir [40]. In the whole horizontal well group, Well 1, Well 4, and Well 5 are located in one formation, while Well 2, Well 3, Well 6, and Well 7 belong to another formation.

In this work, we used data from Well 3 and Well 4 to test our model for the following two reasons. Firstly, the two wells were drilled through the shale gas reservoir in different directions and are located in two different formations. Secondly, microseismic monitoring is conducted in the two wells together with a comprehensive drilling, completion data, and well test data. Figure 2 shows gas and water production rates of the two wells. The two wells both experienced gas breakthrough immediately after well opening and production, meaning that there was no single-phase flow. The difference is that Well 3 experienced a precipitous drop in production at one point (80 hrs), while Well 4 experienced a more gentle fluctuation, possibly due to different formation conditions. We are sorry that there is no further research on the causes of this phenomenon in this paper on account of insufficient high-frequency production data or complete adjacent test well data.

2.2. Producing Gas-Water Ratios (GWR). In order to explore the trend of GWR of production data, this section simply processes and analyzes the production data to observe whether there is an immediate gas breakthrough after the production of shale gas wells [17, 27], which means that SRV can be calculated by establishing relevant models based on production data in this area.

This is largely because the effective fracture network system is saturated with both the gas and water phases after two shut-ins. The gas source here is assumed to be from three aspects: (1) the originally existing initial gas in the active natural fracture, (2) the gas displaced by fracturing fluid under the influence of the strong countercurrent water imbibitions into the shale matrix due to the huge pressure difference during the first shut-in period, and (3) the gas accumulation that resulted from spontaneous imbibitions of fracturing fluid during the second shut-in period [41, 42].

Similarly, before establishing the model, we also need to use the gas-water yield ratio to gain the V-shaped trend. Thus, we processed the initial two-phase production data of Well 3 and Well 4 and finally obtained the trend of the gas-water ratio (GWR). Figure 3 shows a V-shaped trend GWR over time as a feature of early two-phase flowback data. Although the inflection points in the GWR curves of the two wells occur at different times due to different formation conditions and production systems, the same V-shaped trend still appears obviously. Ghanbari et al. [15] and Abbasi [16] also found the V-shaped GWR in the wells drilled in the Horn River shales in Canada.

The gas-water ratio decreases and then increases, and we can study it from the most basic theory. Assume that the gas-water two-phase flow satisfies Darcy's law:

$$Q = -\frac{kA}{\mu}\frac{dP}{dL}, \tag{1}$$

where Q is the fluid flow rate under pressure P, m^3/s; k is the fluid permeability, μm^2; A is the fluid flow area, m^2; μ is the fluid viscosity, mP·s; P is the pressure, MPa; and L is the fluid flow length, m.

After ignoring the capillary force in the fracture network system, the gas-water ratio becomes

$$\frac{q_g}{q_w} = \frac{\mu_w}{\mu_g(P)}\frac{k_{rg}(S_g)}{k_{rw}(S_w)}\frac{\partial P_g}{\partial P_w} \approx \frac{\mu_w}{\mu_g(P)}\frac{k_{rg}(S_g)}{k_{rw}(S_w)}, \tag{2}$$

where q_g and q_w are the flow rates of the gas phase and water phase, respectively, m^3/d; μ_w and $\mu_g(P)$ are the viscosity of the gas phase and water phase under P pressure, respectively, mP·s; $k_{rg}(S_g)$ and $k_{rw}(S_w)$ are the relative permeability of the gas phase and water phase under their respective saturation, μm^2; S_g and S_w are the saturation of the gas phase and water phase, dimensionless; and P_g and P_w are the pressure of the gas phase and water phase, respectively, MPa.

After the well opening for production, the gas viscosity decreases with the decrease of pressure, while the water viscosity remains relatively unchanged. According to the change of the gas-water ratio over time, the ratio of gas-water relative permeability decreases. Therefore, on the basis of the relationship between permeability and saturation, it can be inferred that the saturation ratio has a corresponding variation trend, meaning that the initial gas saturation (S_{gi}) is not zero, which also proves the existence of initial free gas in the fracture before well opening. When the wellbore storage effect disappears, the gas flows from the matrix to the fracture network, resulting in the replenishment of gas in the fracture system. Accordingly, the gas saturation increases, so the gas-water relative permeability increases and the gas-water ratio decreases. This is why the slope of the GWR curve drops first and then rises.

In general, the negative slope on the GWR diagnostic plot is called early gas production (EGP) and the rise of the GWR diagnostic plot is called late gas production (LGP). It is generally believed that the EGP region is the stage of wellbore storage effects and both the gas and water productions come from the effective fracture connected with the horizontal well. Also, the increase of water relative permeability is greater than the reduction of gas viscosity. The LGP phase

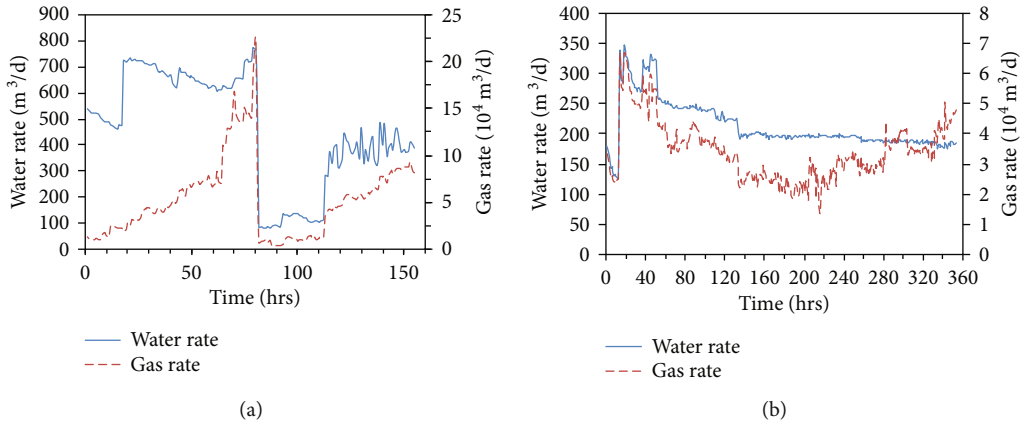

Figure 2: Diagnostic plots for two wells in shale gas formations belonging to southern Sichuan. (a) Production rate plot for Well 3. (b) Production rate plot for Well 4.

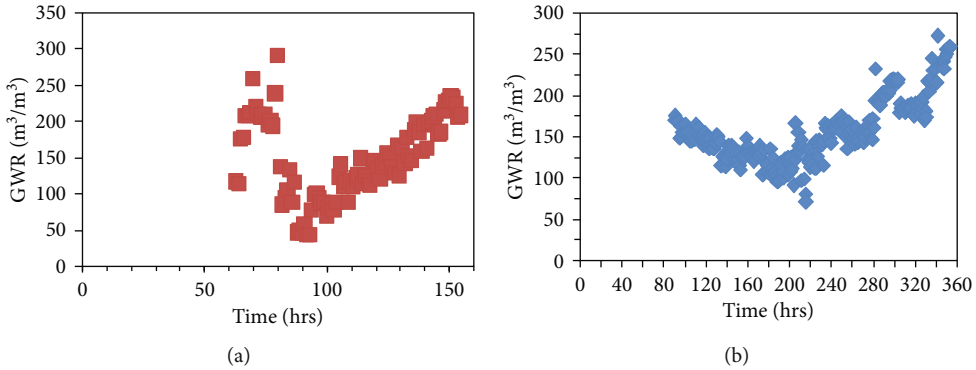

Figure 3: Diagnostic plots for two wells in shale gas formations belonging to southern Sichuan. (a) GWR plot for Well 3. (b) GWR plot for Well 4.

is the result of the matrix gas transfer to the fracture network after wellbore effects becoming negligible [10, 11, 17, 25–27]. According to the above analysis, we have figured out that in the EGP stage, the ground flow of flowback is only from the effective fracture system, while after the LGP stage beginning, the matrix gas initiates participation in the flow. Therefore, we will establish an analysis model for the EGP phase to calculate the SRV of shale gas wells after multistage fracturing.

3. Methods

3.1. Material Balance Equation (MBE) and Diffusion Equation for the Fracture System. In order to facilitate the establishment of the mathematical model for the EGP phase, the fracture network around the shale gas fractured well is simplified into the SRV region composed of the matrix system and fracture system. As shown in Figure 4, the effective fracture system is made up of a fracture section and a matrix section. The fracture section consists of artificial hydraulic fractures, the secondary fractures generated by fracturing, and active natural fractures. The matrix section is the shale matrix connected to the fracture section. It is worth noting that the desorption and adsorption processes were ignored in the material balance equation (MBE) [17, 43].

This model simplifies complex, active natural and secondary fractures, as well as artificial hydraulic fractures, into a simple fracture system. The length of the artificial hydraulic fracture is used as the width of the entire stimulated reservoir volume, and the length of the horizontal wellbore is used as the length. In the whole stimulated reservoir area, the height of the major fracture, including the matrix part connected to the fracture system, participates in the flow. In the equivalent fracture system, the fracture is saturated with fracturing fluid (water phase) and natural gas (gas phase). It is assumed that no matrix gas is involved in the flow during the early gas production (EGP).

It is assumed that the fracture system can be approximated as a homogeneous/closed/tank system. And the fluid flow from the fracture to the horizontal well is assumed to be linear. The mechanism driving the gas-water flow includes two aspects: (1) fracture closure and (2) expansion of the fluid (gas-water phase). Kuchuk et al. [44] also considered the assumption that fracture closure and expansion of water and free gas in the fracture system drive the accumulation of natural gas and water at the surface suggesting the occurrence of pseudo-steady-state flow in fractured reservoirs.

In general, for the purpose of facilitating the establishment and solution of the model, we made the following assumptions: (1) capillary pressure in fracture systems is

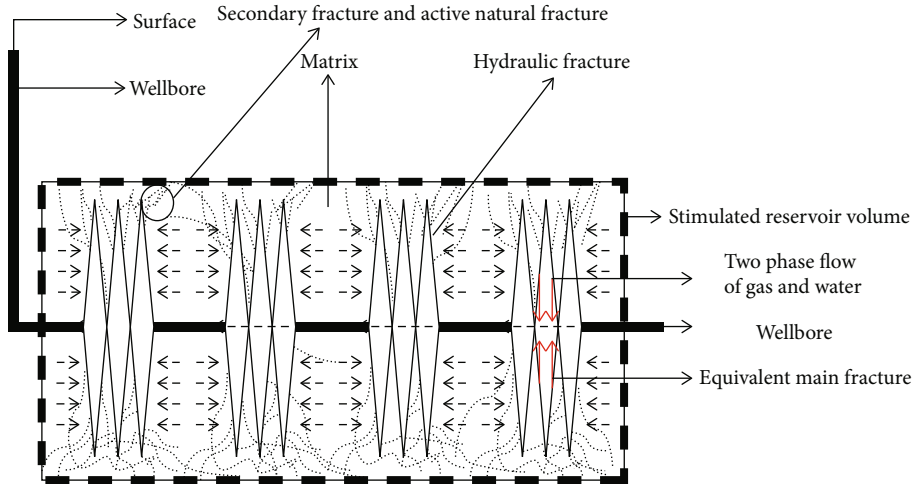

Figure 4: Schematic diagram of the horizontal well with multistage hydraulic fracturing for the development of material balance equation. Dashed arrows show fluid flow direction, which is sequentially from the matrix to fractures and fractures to the wellbore.

ignored; (2) the gas from the matrix is negligible in the EGP stage; (3) the fracture system is approximated as a homogeneous/closed system; (4) Darcy's law applies to fluid flow; and (5) the effective fracture system is saturated with fracturing fluid (water phase) and natural gas (gas phase) initially.

Effective compressibility terms are defined using simplified gas material balance equations (MBEs) [45–48]. In this work, the material balance equation (MBE) of the gas phase in the fracture network is simplified. The effects of gas and water (fracturing fluid) expansion and fracture closure are classified as the "effective compressibility" term given by

$$\tilde{C}_t = \left(1 - \frac{G_p}{G_{fi}}\right)\frac{B_g}{B_{gi}}S_{gi}C_g + \left(1 - \frac{W_p}{W_{fi}}\right)S_{wi}C_w + \frac{1}{V_{fi}}\frac{\partial V_f}{\partial P_f}, \tag{3}$$

where G_p and G_{fi} are the cumulative gas production and initial volume of gas in the fracture, respectively, m^3; B_g and B_{gi} are the gas formation volume factor and gas formation volume factor at initial conditions, respectively, m^3/m^3; S_{gi} and S_{wi} are the initial gas phase saturation and initial water phase saturation, respectively, dimensionless; C_g and C_w are the gas compressibility and water compressibility, respectively, Pa^{-1}; W_p and W_{fi} are the cumulative water production and initial volume of water in the fracture, respectively, m^3; V_f and V_{fi} are the volume of effective fractures and volume of effective fractures at initial conditions, m^3; and P_f is the fracture pressure, Pa.

$\tilde{C}_t$ is analogous to the total compressibility term proposed for conventional multiphase well testing. This is represented as a function of measurable flowback parameters, including cumulative gas production and cumulative water production. Each term in its expression outlines different driving mechanisms in the fracture system: (1) expansion of the gas phase, (2) expansion of liquid phase, and (3) fracture closure. Among them, $(1/V_{fi})(\partial V_f/\partial P_f)$ is similar to the formation compressibility coefficient in traditional conventional material balance analysis [49]. When dealing with fractures, it refers to the inverse of the fracture stiffness determined by the elastic or strain energy required to keep the hydraulic fracture open [50].

Ignoring the gas flow rate from the matrix system to the fracture, the gas phase material balance equation is

$$0 - q_g\rho_g^0 = \frac{\partial}{\partial t}\left[\left(V_g(t)\right)\rho_g^R\right], \tag{4}$$

where $\rho_g{}^0$ and $\rho_g{}^R$ are the density of gas at surface conditions and reservoir conditions, respectively, kg/m^3; and $V_g(t)$ is the volume of gas in the fracture system at any time, m^3.

According to the relationship between gas volume V_g, fracture volume V_f, and water volume V_w in the fracture system, the definition of gas compressibility is obtained as

$$-q_gB_g = V_gc_g\frac{\partial P_f}{\partial t} - \frac{\partial V_w}{\partial t} + \frac{\partial V_f}{\partial t}, \tag{5}$$

where V_f, V_g, and V_w are the fracture volume, gas volume, and water volume in the fracture system, respectively, m^3.

By substituting the gas production G_p and water production W_p, then using the chain rule, the total volume of fractures is derived:

$$-\frac{1}{V_{fi}}\left(q_gB_g + q_wB_w\right) = \frac{\left(G_{fi} - G_p\right)B_gc_g}{G_{fi}B_{gi}/S_{gi}}\frac{\partial P_f}{\partial t} + \frac{\left(W_{fi} - W_p\right)B_wc_w}{W_{fi}B_{wi}/S_{wi}}\frac{\partial P_f}{\partial t} + \frac{1}{V_{fi}}\frac{\partial V_f}{\partial P_f}\frac{\partial P_f}{\partial t}, \tag{6}$$

where B_w is the water formation volume factor at initial conditions, m^3/m^3.

In the early gas production (EGP), it is assumed that $B_w \approx B_{wi}$, the final material balance equation, can be obtained

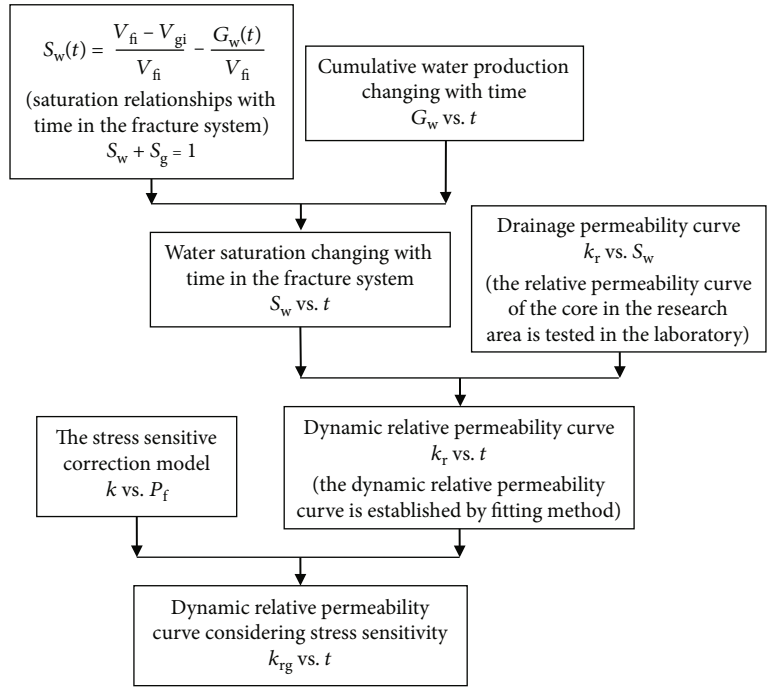

Figure 5: Procedure to estimate the dynamic relative permeability (DRP) curve considering stress sensitivity.

by defining a compressibility term and the total fluid flow rate by simplifying the above equation is

$$\frac{\partial P_f}{\partial t} = -\frac{q_t}{\tilde{C}_t V_{fi}}, \tag{7}$$

where $q_t = q_g B_g + q_w B$ is total producing rate, m^3/d.

Given that single-phase, steady-state flow can be described using the continuity equation and Darcy's law, the single-phase gas diffusion equation in the fracture system is given by Zhang and Winter [51]:

$$\nabla\left[\frac{P_f}{\mu_g Z}\nabla P_f\right] = \frac{\phi_f}{K_f}\frac{P_f}{Z}\tilde{C}_t\frac{\partial P_f}{\partial t}, \tag{8}$$

where Z is the gas compressibility factor, dimensionless; φ_f is the porosity for the fracture system, dimensionless; and ∇ is the gradient operator.

Define the pseudopressure and pseudotime functions [46, 52] as

$$\psi(P_f) = \int_0^{P_f} \frac{2P_f}{\mu_g Z}\partial P_f, \tag{9}$$

$$t_a = \int_0^t \frac{k_g(t)}{\mu_g \tilde{C}_t}\partial t, \tag{10}$$

where $k_g(t)$ is the relative permeability of the gas at a given time, μm^2; and $\tilde{C}_t$ is the total effective compressibility, Pa^{-1}.

Then, the governing equation of single-phase gas flow in the fracture system is

$$\frac{\partial^2 \psi(P_f)}{\partial y^2} = \frac{\phi_f}{K_f}\frac{\partial \psi}{\partial t_a}. \tag{11}$$

3.2. Coupling Stress Sensitivity with Dynamic Relative Permeability Function. In Equation (10), $k_g(t)$ is the variable function of single-phase gas with time. By introducing the dynamic relative permeability (DRP) function $k_{rg}(t)$, the diffusion equation of single-phase gas is transformed into the diffusion equation of the two-phase system [53].

The method in this paper is similar to that in Ezulike and Dehghanpour's study [53], but due to the geological conditions of formations belonging to southern Sichuan being different from those of North America, the dynamic relative permeability (DRP) function of the gas phase is obtained by using the method of fitting field data. In the previous study, we have assumed that the fracture system is saturated with gas and water. The relationship between cumulative gas and water production and time can be reported through field data. Therefore, the gas-water saturation in the fracture system can be established as a function of gas-water production with time. Given the characteristics of abnormal overpressure in this area, the stress sensitivity in this area cannot be ignored [36, 54, 55]. Therefore, the stress-sensitive model was considered in the dynamic relative permeability function. The specific process is shown in Figure 5.

In Figure 6, the relative permeability of the cores after fracturing in the research area is tested through laboratory experiments. The curve of pressure change with time during the flowback period is shown in Figure 7. Stress-strain

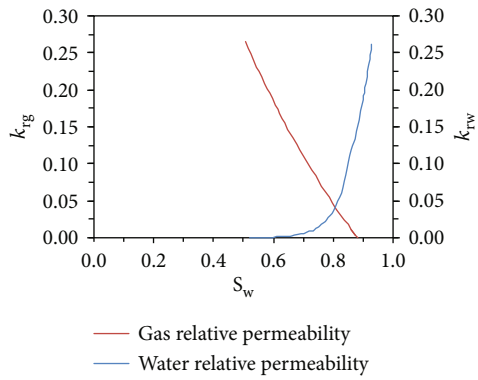

Figure 6: Gas-water relative permeability curve of the cores from Well 3 and Well 4.

experiments were performed to describe the curves between dimensionless permeability and effective stress by stabilizing the confining pressure and reducing the internal pressure. This is more in line with the actual formation flowback pressure changes. The early flowback stage of shale gas wells after well opening is significantly short; therefore, it can be assumed that the formation pressure has not changed much, but the inner pressure begins to decrease after the fluid flows out of the cores.

Take the stress sensitivity experiments of cores belonging to the stimulated area of Well 3 as an example. Both the matrix and the fractures are most likely contained in these cores. We had required as many experiments as possible to obtain the stress-sensitive test data in the stimulated region after fracturing as accurately as possible. However, subject to the insufficient samples or the different distances of samples from the horizontal well, these data maybe cannot represent the whole area in fact but still have considerable reference and research value.

The specific experimental procedures are as follows: (1) the initial confining pressure was set as the original formation pressure which is 38 MPa, and the internal pressure was 23 MPa; (2) the confining pressure was increased to 58 MPa slowly which is the formation pressure before well opening for flowback, and the internal pressure was increased to 43 MPa at the same time to keep the effective stress constant; and (3) the internal pressure was reduced to different pressure points to increase the effective stress, and the gas permeability of the sample was measured after each pressure point was stabilized.

Dimensionless permeability is defined as

$$\frac{K}{K_0} = ae^{-b(p_i - p_f)}, \tag{12}$$

where K is the relative permeability of the gas at a given time, μm^2; K_0 is the initial gas relative permeability, μm^2; and a are b are stress sensitivity coefficients by experiments, dimensionless.

The experimental results are reported in Figure 8. According to the calculation method in Figure 5, the results in Figure 9 were finally obtained. Then, according to the fitting curve, the function of gas-phase relative permeability changing with time is

$$k_{rg}(t) = \alpha t - \beta. \tag{13}$$

Since the above equation is obtained based on flowback data and core experiment relative permeability, α and β are called the flowback data coefficient and flowback data intercept, respectively, which are determined by the data fitting curve.

3.3. Two-Phase Flowback Model for Early Gas Production (EGP). By substituting Equation (13) into Equation (10), the governing equation of single-phase gas flow in the fracture system is changed into the two-phase flow model. This means that when gas-water two-phase flow occurs in the fracture system, the new real pseudotime function is transformed into

$$t_a = \int_0^t \frac{k_{rg}(t)}{\mu_g \tilde{C}_t} \partial t. \tag{14}$$

In order to establish the relationship between pseudopressure function and pseudotime function, we make the following transformation:

$$\frac{\partial \psi}{\partial t_a} = \frac{\partial P_f}{\partial t} \times \frac{\partial \psi}{\partial P_f} \times \frac{\partial t}{\partial t_a}. \tag{15}$$

And $\partial P_f/\partial t$ is derived by the final material balance equation (Equation (7)); in a similar way, we can gain $\partial \psi/\partial P_f$ and $\partial t/\partial t_a$ by the defined pseudopressure (Equation (9)) and new pseudotime equation (Equation (14)), respectively. Finally, Equation (15) becomes

$$\frac{\partial \psi}{\partial t_a} = -\frac{2}{V_{fi}} \frac{q_t}{k_{rg}(t)} \frac{P_f}{Z}. \tag{16}$$

Define the equivalent gas rate as [48]

$$q_g^* = \frac{1}{k_{rg}(t)} \left[q_g B_{gi} + q_w B_w \right]. \tag{17}$$

Substituting P_f/Z in Equation (16) using the real gas law, then combine it with the equivalent gas rate (Equation (17)):

$$\frac{\partial \psi}{\partial t_a} = \left[-\frac{2}{V_{fi}} \frac{P_i}{Z_i} \right] q_g^*. \tag{18}$$

By substituting $\partial \psi/\partial t_a$ (Equation (18)) in Equation (11), we can establish the two-phase diffusion equation:

$$\frac{\partial^2 \psi(P_f)}{\partial y^2} = \frac{\phi_f}{K_f} \left[-\frac{2}{V_{fi}} \frac{P_i}{Z_i} \right] q_g^*. \tag{19}$$

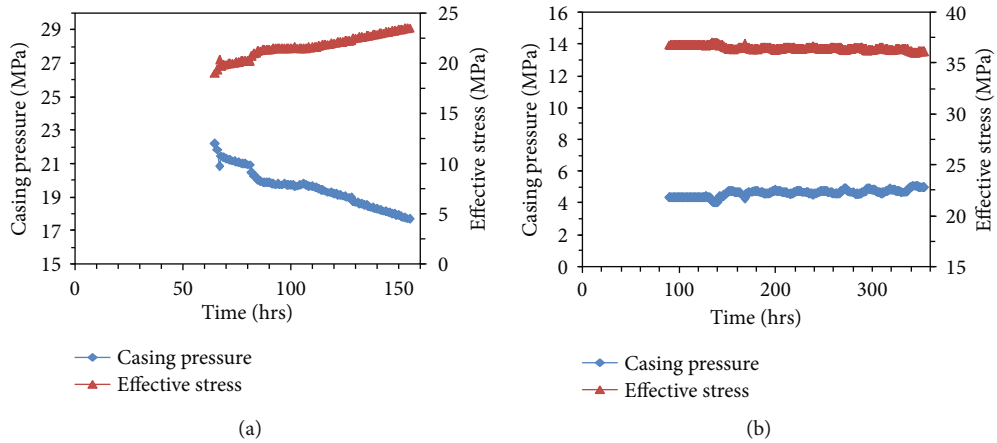

Figure 7: Casing pressure and effective stress changed with time for two wells in shale gas formations belonging to southern Sichuan. (a) Well 3 and (b) Well 4.

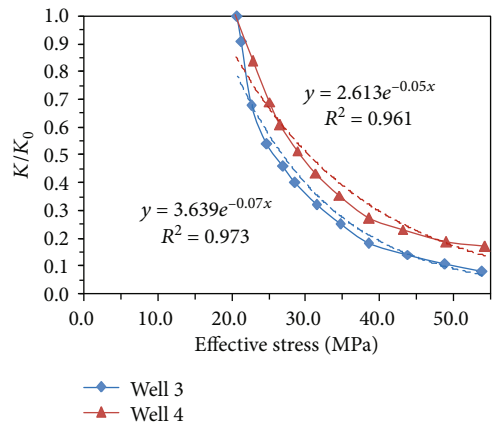

Figure 8: Stress-strain experiment results of Well 3 and Well 4.

Then, the following inner and outer boundary conditions can be solved: $y = Y_e$, $\partial\psi(P_f)/\partial y = 0$, and $y = 0$, $\psi(P_f) = \psi(P_{wf})$.

Define the fracture storage coefficient as

$$C_{st} = \frac{V_{fi} Z_i}{2P_i}. \tag{20}$$

Then, the following relationship is gained:

$$\frac{\psi(\bar{P}_f) - \psi(P_{wf})}{q_g^*} = \frac{\phi_f}{K_f} \frac{1}{C_{st}} \left[\frac{Y_e^2}{3}\right]. \tag{21}$$

Substitute Equation (20) into Equation (18) and integrate to obtain

$$t_a = C_{st} \frac{\psi(P_i) - \psi(\bar{P}_f)}{q_g^*}. \tag{22}$$

By combining Equation (22) with Equation (15), we can modify the final two-phase flow model of the early gas production stage as follows:

$$\left[\frac{\psi(P_i) - \psi(P_{wf})}{q_g^*}\right] = \left[\frac{1}{C_{st}}\right] t_a + \frac{\phi_f}{K_f} \left[\frac{1}{C_{st}}\right] \left[\frac{Y_e^2}{3}\right]. \tag{23}$$

Theoretically, a plot of the rate-normalized pseudopressure (RNP) vs. the pseudotime should yield a straight line relationship. With the pseudotime function as an independent variable and the left side of the equation as a dependent variable, the slope and intercept can be obtained according to the fitting curve, and the relationship between the equivalent fracture porosity/half-length of the effective fracture system and effective fracture system permeability can be described as follows:

$$C_{st} = \frac{1}{\text{slope}} = \frac{V_{fi} Z_i}{2P_i}, \tag{24}$$

$$Y_D = \frac{y\text{-axis intercept}}{\text{slope}} = \frac{\phi_f}{K_f} \left[\frac{Y_e^2}{3}\right]. \tag{25}$$

3.4. Analysis Procedure. We propose the following analysis procedure:

(1) Obtain and process water and gas flowback data to explore a V-shaped gas-water ratio trend (see Figures 2 and 3 and Equation (2))

(2) The early flowback period (EGP) is distinguished from the late flowback period (LGP) according to the V-shaped trend of the GWR curve (see Figure 3)

(3) Conduct a simpler fracture network system model for the EGP (see Figure 4)

(4) Calculate effective compressibility by Equation (3) to deduce the two-phase material balance equation (MBE) (Equation (7)) for the fracture system

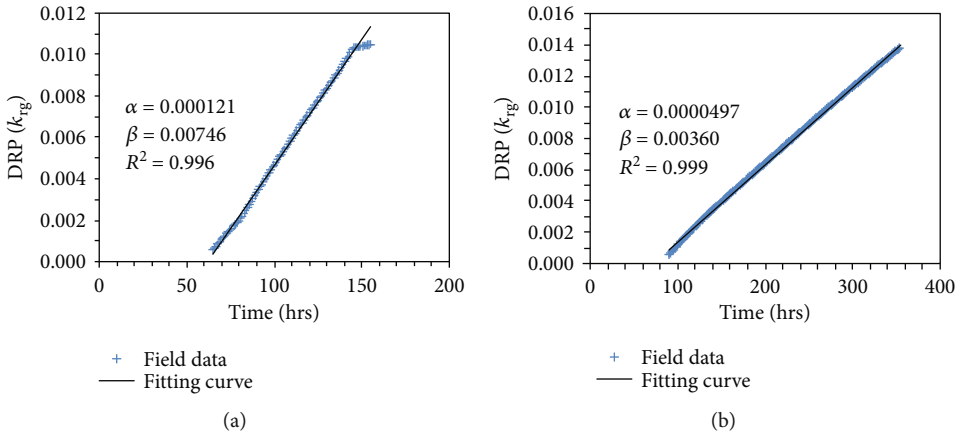

Figure 9: Dynamic relative permeability function over time considering stress sensitivity for two wells in shale gas formations belonging to southern Sichuan. (a) DRP fitting curve for Well 3. (b) DRP fitting curve for Well 4.

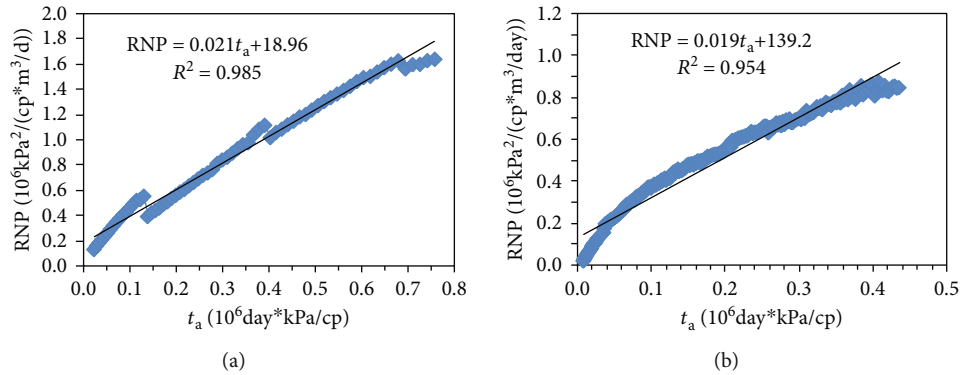

Figure 10: Analysis of EGP data of two wells belonging to southern Sichuan: rate-normalized pressure change with pseudotime. (a) Well 3 and (b) Well 4.

(5) Define the pseudopressure and pseudotime functions (Equations (9) and (10)) to deduce the gas diffusion equation (Equation (11)) of the fracture system

(6) Plot the gas-water relative permeability curve (see Figure 5) and the curves of dimensionless permeability with effective stress (see Figure 8) by experiments

(7) Calculate gas DRP coupling stress sensitivity (see Figure 9) following the steps by Figure 6 to transform the gas diffusion equation (Equation (11)) into the two-phase diffusion equation (Equation (19))

(8) Modify the final two-phase flow mode (Equation (23)) by combining Equation (22) with Equation (15)

(9) Plot rate-normalized pressure change with pseudotime (see Figure 10)

(10) Calculate SRV by Equation (24) and effective fracture system permeability by Equation (25)

(11) Verify the analytical model against microseismic data (see Figure 11)

The flowback data we need to obtain include production rates and pressure and cumulative production data profiles. Then, we got a V-shaped trend in the gas-water ratio curve by processing the flowback data. Thus, an analytical model was established for the EGP stage. Finally, the calculated results were compared with the microseismic data to validate the mathematical results.

4. Results and Discussions

4.1. Stimulated Reservoir Volume. We apply the analytical model presented above to analyze the flowback data of Well 3 and Well 4. However, there are several issues that need to be addressed and discussed:

(1) It is difficult to gain an appropriate initial gas saturation of the fracture system from actual field data. Unlike conventional numerical simulation, this parameter is unknown in actual field data. After the

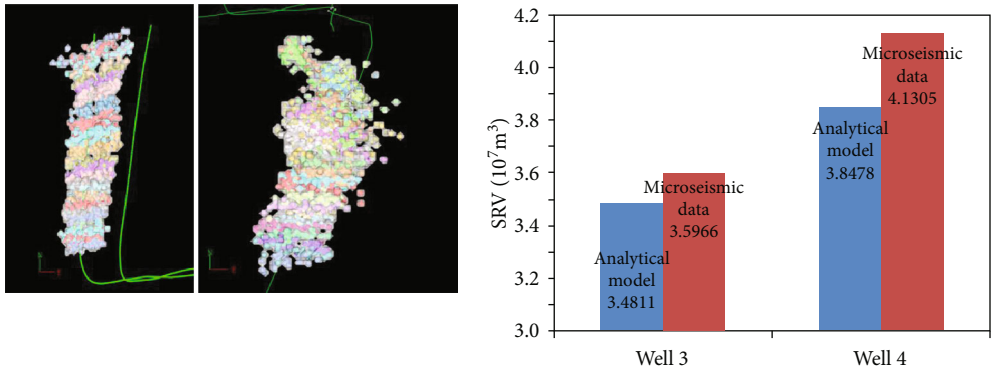

Figure 11: (a) Renderings of microseismic detection technology for Well 3 and Well 4. (b) Comparison between the analytical model and the microseismic data.

fracturing operation is completed, the effective fracture system connecting the wellbore is filled with fracturing fluid approximately. Thus, after the well is opened for flowback operation and before production, the volume of the recovered fracturing fluid under the ground is filled with gas renewedly. Therefore, in this paper, we take a reasonable value which is the recovery percentage of the total injection amount of fracturing fluid as the initial fracture system gas saturation in calculation. According to Xu's paper [48], there is a little significant difference between the actual value of initial gas saturation and the recovery percentage. However, this was still not rigorous enough. Then, other possible values are substituted into the calculation by us to get the new SRV. The results showed that the impact of this value on SRV estimation was not obvious within the error range, and the difference was less than 1% compared with the microseismic data

Due to that, fracturing fluid may leak off into the existing inactive natural fractures and into the matrix during injection; the fluid flowback percentage decreases, but the initial gas saturation in the fracture system increases. Hence, when a significant portion of the injected fluid volume does not contribute to create fracture volume, this value of the initial gas saturation for calculation is actually low. One direction of future work is to consider using the results to iteratively optimize the initial gas saturation value.

(2) The value of the fracture closure term in the total compressibility cannot be accurately expressed. Fortunately, it is found that this value has no obvious influence on the results in the calculation process. Since this value refers to the inverse of fracture stiffness when dealing with fractures, it is considered to give a reasonable value in the subsequent work from the perspective of rock fracture mechanics

The final model calculation results are shown in Figure 10. Since microseismic detection technology was used to estimate the final hydraulic fracture stimulated effect in the two wells. We compared the calculated results with the microseismic data and finally found that the difference between the calculated results of the analytical model and the microseismic data was minor, as shown in Figure 11. This reason is that quantities of fractures that do not connect effectively with fracture systems are counted in the final result when microseismic detection techniques are used. Those "dead" fractures skew the microseismic results.

4.2. Effective Fracture System Permeability of Stimulated Reservoir. As shown in Table 1, after obtaining the slope of rate-normalized pressure change with pseudotime (see Figure 10), SRV was gained by Equation (17). On the basis of the average length of hydraulic fractures provided by the microseismic data of the drilling platform where Well 3 and Well 4 are located and the average porosity of the cores after fracturing obtained through experiments, the permeability of the effective fracture system in the stimulated region is calculated by using Equation (18). The results are shown in Table 1, where the absolute deviation refers to the difference between the SRV calculated by the analytical model and estimated by the microseismic data, and the relative deviation refers to the ratio of the absolute deviation to the SRV estimated by microseismic data. Numerical errors in porosity of the effective fracture system are responsible for the error of permeability.

If the SRV estimated by microseismic data is taken as a reference for comparison, the specific calculation process is as follows:

$$d_A = V_A - V_M, \tag{26}$$

$$d_R = \frac{(V_A - V_M)}{V_M}, \tag{27}$$

where d_A and d_R are the absolute deviation and the relative deviation between the SRV calculated by the analytical model and estimated by the microseismic data, respectively, m^3; and V_A and V_M are the SRV calculated by the analytical model and the SRV estimated by the microseismic data, m^3.

Table 1: Different results of the analytical model and microseismic data.

Parameter name	Well 3	Well 4
SRV calculated by the analytical model	3.4811×10^7 m^3	3.8478×10^7 m^3
SRV estimated by the microseismic data	3.5966×10^7 m^3	4.1305×10^7 m^3
The absolute deviation	1.1150×10^6 m^3	2.8270×10^6 m^3
The relative deviation	3.2%	6.8%
Effective fracture system permeability	0.301 mD	0.244 mD
Average half-length of hydraulic fractures	320 m	285 m
Effective fracture system porosity	15.5%	13.8%

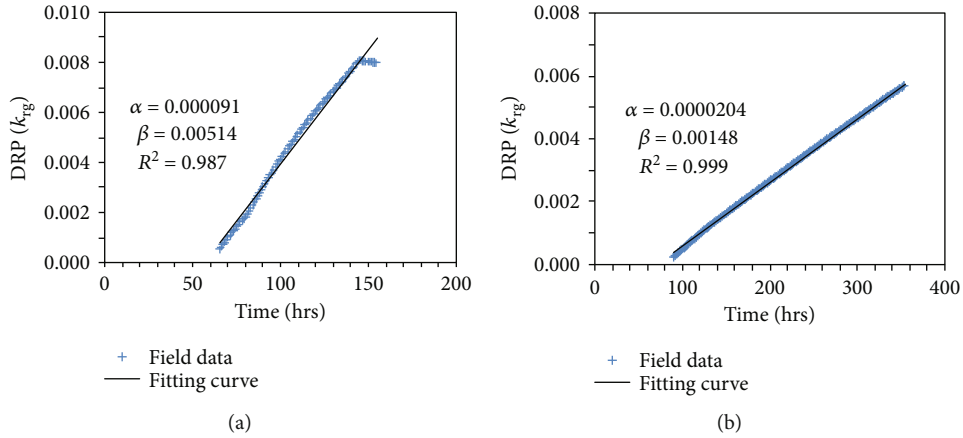

Figure 12: Dynamic relative permeability function over time without stress sensitivity for two wells belonging to southern Sichuan. (a) DRP for Well 3. (b) DRP for Well 4.

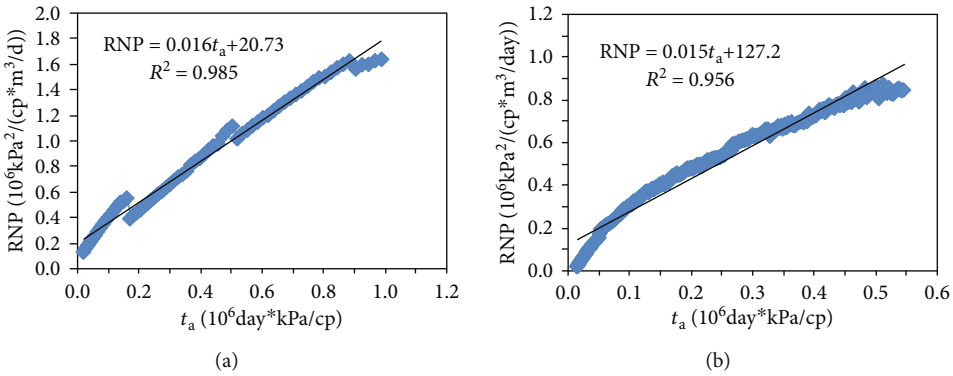

Figure 13: Analysis without considering stress sensitivity of EGP data of two wells in shale gas belonging to southern Sichuan: rate-normalized pressure change with pseudotime. (a) Well 3 and (b) Well 4.

4.3. Analytical Model without Considering Stress Sensitivity. If the stress sensitivity effect is not considered in the process of the DRP calculation, the deviation of the DRP curve will occur, as shown in Figure 12. And the curve with a large error was substituted into the step shown in Section 3.4 to get the result in Figure 13. As a result, both the slope and the intercept of the RNP curve had changed. We obtained the new slope and intercept of the curve and calculated a new SRV according to Equations (17) and (18). Then, the calculation results and corresponding deviations as shown in Figure 14 were obtained.

It can be seen that the relative deviation calculated without considering the stress sensitivity effect is greater than that calculated with considering the stress sensitivity effect. Moreover, because the real SRV has been overestimated by the microseismic data, the calculation results of the model without considering the stress sensitivity effect are higher than those of the microseismic data, which further indicates that the calculation results without considering the stress sensitivity effect in the high-pressure area will have a large error, which cannot be ignored. We also calculated the permeability of the effective fracture system, and the effective permeability

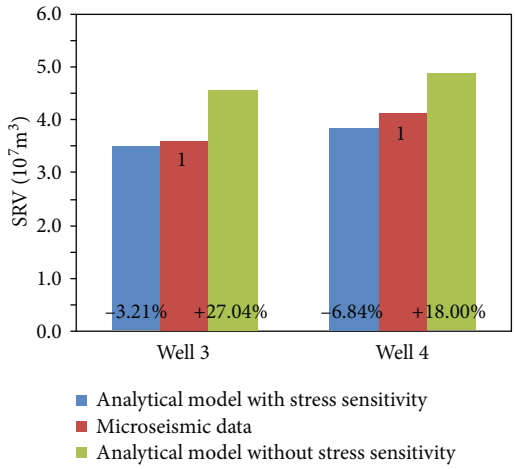

Figure 14: Comparison between the analytical model with or without considering stress sensitivity and the microseismic data.

of Well 3 and Well 4 was 0.432 mD and 0.283 mD, respectively. It can be seen that the calculation results are 43.50% and 15.75% more than those considering the stress sensitivity effect.

5. Conclusions

In this paper, a comprehensive model is developed to predict SRV in the shale gas reservoirs using the flowback data after fracturing. The stress sensitivity is included as well. The results of SRV are compared with the microseismic data. The following conclusions can be drawn:

(1) The flowback data show that the gas-water ratio is V-shaped, i.e., the early descending stage and the late ascending stage in this field, which can be used to estimate the volume of the effective fracture system

(2) The stress sensitivity is a key factor affecting the permeability of the effective fracture system as well as the SRV in the shale gas reservoirs. Once it is neglected, the estimation will be overestimated

(3) Stress sensitivity is taken into account to forecast SRV in this typical block. Results show that the relative deviation of stimulated reservoir volume calculated by this proposed model and the microseismic data is less than 10%, indicating that this method could provide reasonable prediction

Data Availability

The test data used to support the findings of this study are included within the article. Readers can obtain data supporting the research results from the test data table in the paper.

Conflicts of Interest

The authors declare that there is no conflict of interest regarding the publication of this paper.

Acknowledgments

This research was funded by the National Science and Technology Major Project of China (2017ZX05009-005), Fundamental Research Funds for the Central Universities (2652018209), and National Natural Science Foundation of China (51804282).

References

[1] G. Wang, A. Jia, Y. Wei, and C. Xiao, "Transient pressure analysis for multifractured horizontal well with the use of multilinear flow model in shale gas reservoir," *Geofluids*, vol. 2020, Article ID 8348205, 20 pages, 2020.

[2] W. Zhou, R. Banerjee, B. D. Poe, J. Spath, and M. Thambynayagam, "Semianalytical production simulation of complex hydraulic-fracture networks," *SPE Journal*, vol. 19, no. 1, pp. 6–18, 2014.

[3] C. E. Neuzil, "How permeable are clays and shales?," *Water Resources Research*, vol. 30, no. 2, pp. 145–150, 1994.

[4] R. S. Jones Jr., B. Pownall, and J. Franke, "Estimating reservoir pressure from early flowback data," in *Unconventional Resources Technology Conference*, pp. 25–27, Denver, Colorado, August 2014.

[5] B. Zanganeh, M. Soroush, J. D. Williams-Kovacs, and C. R. Clarkson, "Parameters affecting load recovery and oil breakthrough time after hydraulic fracturing in tight oil wells," in *SPE/CSUR Unconventional Resources Conference*, pp. 20–22, Calgary, Alberta, October 2015.

[6] A. Mohammadnejad, R. F. Shelley, L. V. Lehman, K. Shah, D. Gusain, and M. T. Conway, "Development of the brittle shale fracture network model," in *SPE Hydraulic Fracturing Technology Conference*, pp. 4–6, The Woodlands, Texas, USA, February 2013.

[7] J. Xu, C. Guo, W. Teng, M. Wei, and R. Jiang, "Production performance analysis of tight oil/gas reservoirs considering stimulated reservoir volume using elliptical flow," *Journal of Natural Gas Science and Engineering*, vol. 26, pp. 827–839, 2015.

[8] M. Wu, M. Ding, J. Yao, S. Xu, L. Li, and X. Li, "Pressure transient analysis of multiple fractured horizontal well in composite shale gas reservoirs by boundary element method," *Journal of Petroleum Science and Engineering*, vol. 162, pp. 84–101, 2018.

[9] Z. Chen, X. Liao, X. Zhao, W. Yu, and K. Sepehrnoori, "A workflow based on a semianalytical model to estimate the properties of stimulated reservoir volume of tight-oil wells," *Journal of Petroleum Science and Engineering*, vol. 178, pp. 892–903, 2019.

[10] D. Ilk, D. M. Anderson, G. W. J. Stotts, L. Mattar, and T. A. Blasingame, "Production-data analysis, pitfalls, diagnostics," *SPE Resrervoir Evaluation & Engineering*, vol. 13, no. 3, pp. 538–552, 2013.

[11] D. Ilk, S. M. Currie, D. Symmons, J. A. Rushing, N. J. Broussard, and T. A. Blasingame, "A comprehensive workflow for early analysis and interpretation of flowback data from wells in tight gas/shale reservoir systems," in *SPE Annual Technical Conference and Exhibition*, pp. 19–22, Florence, Italy, September 2010.

[12] M. A. Abbasi, H. Dehghanpour, and R. V. Hawkes, "Flowback analysis for fracture characterization," in *SPE Canadian*

Unconventional Resources Conference, Calgary, Alberta, November 2012.

[13] M. A. Abbasi, D. O. Ezulike, H. Dehghanpour, and R. V. Hawkes, "A comparative study of flowback rate and pressure transient behavior in multifractured horizontal wells completed in tight gas and oil reservoirs," *Journal of Natural Gas Science and Engineering*, vol. 17, no. 2, pp. 82–93, 2014.

[14] Y. Zhang and C. Ehlig-Economides, "Accounting for remaining injected fracturing fluid in shale gas wells," in *SPE/AAPG/SEG Unconventional Resources Technology Conference*, pp. 25–27, Denver, Colorado, USA, August 2014.

[15] E. Ghanbari, D. Bearinger, M. A. Abbasi, and H. Dehghanpour, "Flowback volumetric and chemical analysis for evaluating load recovery and its impacton on early-time production," in *SPE Unconventional Resources Conference Canada*, pp. 5–7, Calgary, Alberta, Canada, November 2013.

[16] M. A. Abbasi, *A comparative study of flowback rate and pressure transient behavior in multi-fractured horizontal wells, [Ph.D. thesis]*, University of Alberta, Edmonton, Alberta, Canada, 2013.

[17] C. R. Clarkson, "Modeling two-phase flowback of multifractured horizontal wells completed in shale," in *SPE Canadian Unconventional Resources Conference*, Calgary, Alberta, Canada, November 2012.

[18] J. D. Williams-Kovacs and C. R. Clarkson, "Modeling of two-phase flowback from multi-fractured horizontal tight gas wells stimulated with nitrogen energized frac fluid," in *SPE Unconventional Resource Conference Canada*, Calgary, Alberta, November 2013.

[19] Z. Tao, L. Xiangfang, Y. Lifeng, L. Jing, W. Yonghui, and F. Dong, "Effects of shut-in timing on flowback rate and productivity of shale gas wells," *Natural Gas Industry*, vol. 37, no. 8, pp. 48–60, 2017.

[20] O. A. Adefidipe, Y. Xu, H. Dehghanpour, and C. J. Virues, "Immediate gas production from shale gas wells: a two-phase flowback model," in *SPE Unconventional Resources Conference-USA*, The Woodlands, Texas, April 2014.

[21] O. A. Adefidipe, Y. Xu, H. Dehghanpour, and C. J. Virues, "Estimating effective fracture volume from early-time production data: a material balance approach," in *SPE/CSUR Unconventional Resources Conference-Canada*, Calgary, Alberta, October 2014.

[22] Y. Xu, O. A. Adefidipe, and H. Dehghanpour, "Volumetric analysis of two-phase flowback fata for fracture characterization," in *SPE Western Regional Meeting*, Garden Grove, California, April 2015.

[23] Y. Xu, Y. Fu, D. O. Ezulike, H. Dehghanpour, and C. J. Virues, "Modeling two-phase flowback data using an open tank model," in *SPE/CSUR Unconventional Resources Conference*, Calgary, Alberta, October 2015.

[24] D. O. Ezulike, H. Dehghanpour, and R. V. Hawkes, "Understanding flowback as a transient two-phase displacement process: an extension of the linear dual-porosity model," in *CPR Unconventional Resources Conference-Canada*, Calgary, Alberta, November 2013.

[25] D. O. Ezulike and H. Dehghanpour, "A workflow for flowback data analysis–creating value out of chaos," in *2014 Unconventional Resources Technology Conference*, Denver, Colorado, August 2014.

[26] D. O. Ezulike, H. Dehghanpour, and C. J. Virues, "A flowback-guided approach for production data analysis on tight reservoirs," in *2014 SPE/CSUR Unconventional Resources Conference-Canada*, Calgary, Alberta, October 2014.

[27] C. R. Clarkson and J. D. Williams-Kovacs, "A new method for modeling multi-phase flowback of multi-fractures horizontal tight oil wells to determine hydraulic fracture properties," in *SPE Annual Technical Conference and Exhibition*, New Orleans, Louisiana, October 2013.

[28] C. R. Clarkson, F. Qanbari, and J. D. Williams-Kovacs, "Innovative use of rate-transient analysis methods to obtain hydraulic-fracture properties for low-permeability reservoirs exhibiting multiphase flow," *Leading Edge*, vol. 33, no. 10, pp. 1108–1122, 2014.

[29] J. D. Williams-Kovacs and C. R. Clarkson, "Stochastic modeling of multi-phase flowback from multi-fractured horizontal tight oil wells," in *SPE Unconventional Resource Conference–Canada*, Calgary, Alberta, November 2013.

[30] J. D. Williams-Kovacs and C. R. Clarkson, "Stochastic modeling of two-phase flowback of multi-fractured horizontal wells to estimate hydraulic fracture properties and forecast production," in *SPE Unconventional Resource Conference USA*, The Woodlands, Texas, April 2013.

[31] J. D. Williams-Kovacs and C. R. Clarkson, "A modified approach for modeling two-phase flowback from multi-fractured horizontal shale gas wells," in *Unconventional Resources Technology Conference*, San Antonio, Texas, July 2015.

[32] J. D. Williams-Kovacs and C. R. Clarkson, "A modified approach for modeling two-phase flowback from multi-fractured horizontal shale gas wells," *Journal of Natural Gas Science and Engineering*, vol. 30, pp. 127–147, 2016.

[33] Y. Fu, D. O. Ezulike, and H. Dehghanpour, "Estimating effective fracture pore-volume from early single-phase flowback data and relating it to fracture design parameters," in *SPE/CSUR Unconventional Resources Conference*, Calgary, Alberta, October 2015.

[34] A. B. Alkouh, S. McKetta, and R. A. Wattenbarger, "Estimation of effective-fracture volume using water-flowback and production data for shale-gas wells," *Journal of Canadian Petroleum Technology*, vol. 53, no. 5, pp. 293–303, 2014.

[35] X. Wang, Y. Zhu, and C. Fu, "Experimental investigation of the stress-dependent permeability in the Longmaxi Formation shale," *Journal of Petroleum Science and Engineering*, vol. 175, pp. 932–947, 2019.

[36] X. Yan, J. Sun, and D. Liu, "Numerical simulation of shale gas multiscale seepage mechanism-coupled stress sensitivity," *Journal of Chemistry*, vol. 2019, Article ID 7387234, 13 pages, 2019.

[37] W. Liu, J. Liu, M. Cai, C. Luo, X. Shi, and J. Zhang, "Pore evolution characteristic of shale in the Longmaxi Formation, Sichuan Basin," *Petroleum Research*, vol. 2, no. 4, pp. 291–300, 2017.

[38] S. Chen, Y. Zhu, S. Chen, Y. Han, and C. Fu, "Hydrocarbon generation and shale gas accumulation in the Longmaxi Formation, Southern Sichuan Basin, China," *Marine and Petroleum Geology*, vol. 86, pp. 248–258, 2017.

[39] C. Wang, B. Zhang, Y. Lu et al., "Lithofacies distribution characteristics and its controlling factors of shale in Wufeng Formation-Member 1 of Longmaxi Formation in the Jiaoshiba area," *Petroleum Research*, vol. 3, no. 4, pp. 306–319, 2018.

[40] T. Dong, S. He, M. Chen et al., "Quartz types and origins in the paleozoic Wufeng-Longmaxi Formations, Eastern Sichuan

Basin, China: implications for porosity preservation in shale reservoirs," *Marine and Petroleum Geology*, vol. 106, pp. 62–73, 2019.

[41] Y. Cheng, "Impact of water dynamics in fractures on the performance of hydraulically fractured wells in gas-shale reservoirs," *Journal of Canadian Petroleum Technology*, vol. 51, no. 2, pp. 143–151, 2013.

[42] J. Zhang, A. Kamenov, A. D. Hill, and D. Zhu, "Laboratory measurement of hydraulic-fracture conductivities in the Barnett shale," *SPE Production & Operations*, vol. 29, no. 3, pp. 216–227, 2014.

[43] L. Fan, J. W. Thompson, and J. R. Robinson, "Understanding gas production mechanism and effectiveness of well stimulated in the Haynesville shale through reservoir simulation," in *SPE Unconventional Resources & International Petroleum Conference*, Calgary, Alberta, October 2010.

[44] F. J. Kuchuk, D. Biryukov, and T. Fitzpatrick, "Rate transient and decline curve analyses for continuously (dual-porosity) and discretely naturally fractured reservoirs," in *SPE Annual Technical Conference and Exhibition*, Amsterdam, Netherlands, October 2014.

[45] N. M. A. Rahman, L. Kok, and K. Zaoral, "A new method for computing pseudo-time for real gas flow using the material balance equation," *Journal of Canadian Petroleum Technology*, vol. 45, no. 10, pp. 36–44, 2006.

[46] S. Moghadam, O. Jeje, and L. Mattar, "Advanced gas material balance in simplified format," *Journal of Canadian Petroleum Technology*, vol. 50, no. 1, pp. 90–98, 2013.

[47] V. K. Singh, "Overview of material balance equation (MBE) in shale gas & non-conventional reservoir," in *SPE Middle East Oil and Gas Show and Conference*, Manama, Bahrain, March 2013.

[48] Y. Xu, O. A. Adefidipe, and H. Dehghanpour, "A flowing material balance equation for two-phase flowback analysis," *Journal of Petroleum Science & Engineering*, vol. 142, pp. 170–185, 2016.

[49] J. C. Martin, "Simplified equations of flow in gas drive reservoirs and the theoretical foundation of multiphase pressure build up analyses," *Transactions of the AIME*, vol. 216, no. 1, pp. 321–323, 2013.

[50] D. P. Craig, *Analytical modeling of a fracture-injection/fall-off sequenceand the development of a refracture candidate diagnostic test, [Ph.D. thesis]*, Texas A&M University, College Station, Texas, 2006.

[51] D. Zhang and C. Winter, "Moment-equation approach to single phase fluid flow in heterogeneous reservoirs," *SPE Journal*, vol. 4, no. 2, pp. 118–127, 1999.

[52] S. H. Tabatabaie, L. Mattar, and M. Pooladi-Darvish, "Pseudo-time calculationin low permeability gas reservoirs," in *SPE Unconventional Resources Conference Canada*, Calgary, Alberta, Canada, November 2013.

[53] D. O. Ezulike and H. Dehghanpour, "Modelling flowback as a transient two-phase depletion process," *Journal of Natural Gas Science and Engineering*, vol. 19, pp. 258–278, 2014.

[54] Y. Zhao, Z. Wang, X. Qin, J. Li, and H. Yang, "Stress-dependent permeability of coal fracture networks: a numerical study with lattice Boltzmann method," *Journal of Petroleum Science and Engineering*, vol. 173, pp. 1053–1064, 2019.

[55] Z. Ru, K. An, and J. Hu, "The impact of sulfur precipitation in developing a sour gas reservoir with pressure-sensitive effects," *Advances in Geo-Energy Research*, vol. 3, no. 3, pp. 268–276, 2019.